Proceedings of CECNet 2022
A.J. Tallón-Ballesteros (Ed.)

doi:10.3233/FAIA220526

A Method for Power Amplifier Distortions Compensation at the RX Side for the 5G NR Communication Systems

Alexander MALTSEV[a,1], Alexander SHIKOV[b], Andrey PUDEEV[b], Seonwook KIM[c] and Suckchel YANG[c]
[a] *Nizhny Novgorod State University, Nizhny Novgorod, Russia*
[b] *LG Electronics Russia R&D Lab, Moscow, Russia*
[c] *LG Electronics, Seoul, Korea*

Abstract. For the past years, the Internet of Things (IoT) supported by 5G technology, has been expanding rapidly across a wide range of services, enabling inter-object connectivity for the automotive industry, consumer electronics, transportation, logistics sectors, and manufacturing. With the increasing ubiquitous usage of various small-sized sensors, manufacturing cost of each element taken remains a critical aspect. Relatively low price of individual elements is the key for enabling tightly connected environment, but may severely affect RF chains quality as well as overall performance. With 5G expansion to the sub-THz bands, power amplifier nonlinearity may significantly limit system performance even in high-grade devices, due to power amplifier design limitations. Multiple studies were done to mitigate nonlinearity impact, both at the transmitter (TX) and receiver (RX) sides. Many solutions propose for evaluation and further compensation of the PA nonlinearity effects, via decision-directed feedback, training or even statistical processing of the received signal. However, with knowledge of the PA nonlinearity function at the receiver side, the processing may be simplified by the application of the reverse function to the equivalent signal in the time domain. In this paper we propose a method for PA nonlinear distortion compensation at the RX side, which can be adjusted for several signal waveforms adopted in 5G NR (New Radio) standard, such as CP-OFDM, DFT-S-OFDM, and others. The simulation results presented demonstrate performance improvement both for the sub-THz PA models and models for the 30-70 GHz band.

Keywords. 5G NR, OFDM, DFT-s-OFDM, mmWave, subTHz, power amplifier nonlinearity, PA models, PA pre-distortion

1. Introduction

Previous releases of the 5G New Radio (NR) standards Rel.15 and Rel.16 support carrier frequencies up to 52.6 GHz. Considering operations above 52.6 GHz in the next release of the 5G NR standard Rel.17, third generation partnership project (3GPP) radio access network (RAN) specification group already has investigated requirements for 52.6 GHz - 114.25 GHz [1] frequency band, with the main interest to first extend the current NR frequency range 2 (FR2) support to the frequency range 52.6 GHz - 71

[1] Corresponding author: Alexander Maltsev, e-mail: maltsev@rf.unn.ru. This work was partially supported by the Advanced School of Engineering of the Nizhny Novgorod State University.

GHz, with minimal changes to the system [2, 3]. Also, the possibilities of further expansion into the sub-THz band around 71-114 GHz have been considered. In this frequency band, despite recent technology advances in the PA design, they still demonstrate highly non-linear behavior for the typical allowed TX power [4]. Thus, PA distortions may become a significant performance limiting factor, especially for the highly efficient modulations like 64- and 256-QAM.

2. Problem and Previous Solutions

In the lower 5G NR frequency range 1 (FR1) below 6 GHz, and, partially, FR2, the effects of the PA can be neglected in most cases since the PA operation point may be safely placed in the linear region with minimal transmitted signal distortions. However, the problem of the PA nonlinearity distortion compensation may be very important for cheap transceivers with low-quality PA chains. It should be noted that the number of such devices can be very large, since cheap devices are a substantial part of Internet-of-Things (IoT) infrastructure. Therefore, this problem was addressed in a number of works [5-11], even for the lower bands.

In all these works, the Rapp model [12] of the power amplifier nonlinearity is widely used for description of the amplitude and phase distortions of the solid state power amplifiers (SSPA). In the 3GPP specification [1], the modified Rapp PA model, described by the equations shown in Eq. (1), was agreed as the baseline model in the 3GPP specification for simulations.

$$F_{AM-AM}(x) = \frac{Gx}{\left(1+\left|\frac{Gx}{V_{sat}}\right|^{2p}\right)^{1/2p}}, F_{AM-PM}(x) = \frac{Ax^q}{\left(1+\left(\frac{x}{B}\right)^q\right)}, \quad (1)$$

where $F_{AM-AM}(x), F_{AM-PM}(x)$ are the amplitude-to-amplitude and amplitude-to-phase distortions, respectively, G is the small signal gain, p is the smoothness factor and V_{sat} is the saturation voltage. Coefficients A, B, q are phase distortion curve parameters.

Baseline characteristics of the typical power amplifiers in the 30-70 GHz bands were used to derive the PA model [13], viable in the corresponding bands. However, as it can be seen from the recent works [4, 14, 15], the sub-THz PA characteristics in 100-200 GHz bands are different. To evaluate the performance of the mobile communication systems in sub-THz, we have extracted parameters G, p, V_{sat} from the available experimental data [4, 14, 15] by fitting it with the Rapp AM-AM distortion model from Eq. (1). Then we derived a common PA model for 100-200 GHz bands by averaging these parameters. The $F_{AM-AM}(x)$ function for this sub-THz PA model and experimental curves from recent papers are presented in Figure 1. For comparison, the standard PA model used in the 30-70 GHz band is also shown in Figure 1. It can be seen that for the sub-THz PA model, the saturation voltage V_{sat} is about 3-4 dB less than for PA model used in the 30-70 GHz bands.

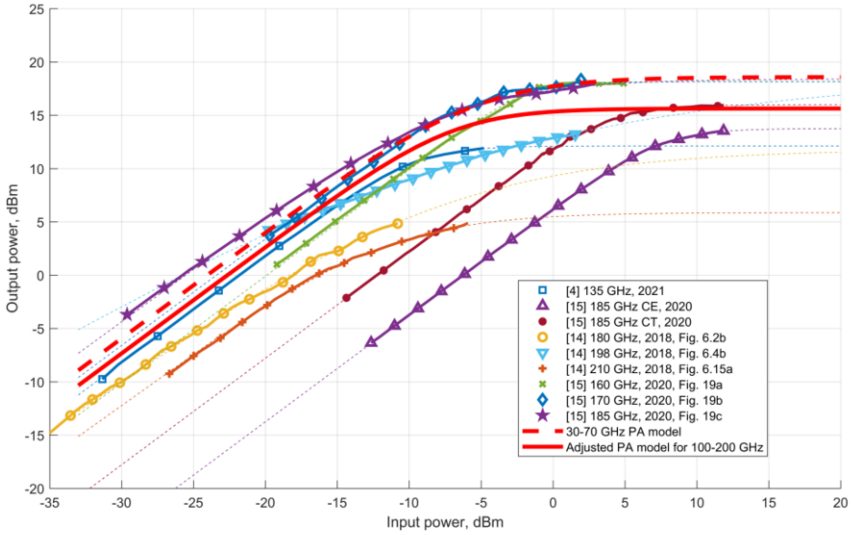

Figure 1. Comparison of SSPA characteristics based on the recent research papers. Dashed lines of the same color as the markers are curve fits of Rapp AM-AM distortion model in Eq. (1).

More detailed PA characteristics in sub-THz band (100-200 GHz), such as used technology, carrier frequency f_c, gain, bandwidth (BW), saturation power P_{sat} and power-added efficiency (PAE), available from literature and evaluated Rapp models parameters are presented in Table 1.

Table 1. Power amplifiers in sub-THz band (100-200GHz).

Parameters Source	Technology	f_c, GHz	Gain, dB	BW, GHz	P_{sat}, dBm	PAE, %	Rapp G	Rapp V_{sat}	Rapp p
[4]	28-nm CMOS	135	21.9	20	11.8	10.7	*12.26*	*0.9*	*1.93*
[14] Fig 6.2b	35-nm mHEMT	180	28	60	--	3.3	*10.84*	*0.87*	*0.52*
[14] Fig 6.4b	50-nm mHEMT	198	13.4	70	--	5	*41.19*	*1.99*	*0.26*
[14] Fig 6.15a	35 nm GaAs mHEMT	210	22.7	~100	--	6.4	*7.89*	*0.44*	*0.9*
[15] CT	130-nm SiGe BiCMOS CT	185	12.3	27	15.8	19.6	*2.05*	*1.09*	*2.031*
[15] CE	130-nm SiGe BiCMOS CE	185	6.3	27	13.5	20	*4.08*	*1.41*	*1.91*
[15] Fig. 19a	130-nm SiGe BiCMOS 3-stage CT	160	20.2	27	18.7	~3.9	*9.88*	*1.81*	*2,75*

[15] Fig. 19b	130-nm SiGe BiCMOS 3-stage CT	170	18.7	27	18.7	4.4	*14.8*	*1.81*	*1.56*
[15] Fig. 19c	130-nm SiGe BiCMOS 3-stage CT	185	25.9	27	18.7	3.5	*19.29*	*1.86*	*0.87*
100-200 GHz PA model	N/A	100-200	13.6	>20	15	3-20	*13.59*	*1.35*	*1.41*
30-70 GHz PA model	N/A	30-70	--	--	--	--	*16*	*1.9*	*1.1*

Figure 2 shows the effect of the PA nonlinearity impact on the different signal waveforms. It can be seen that for a single carrier (SC) system the effect is a straightforward amplitude distortion, which can easily be compensated. On the contrary, for OFDM symbols, PA nonlinearity causes inter-carrier interference (ICI), which is random and cannot be compensated easily at the RX side.

DFT spread OFDM (DFT-s-OFDM) modulation represents an intermediate case, where both deterministic and random components exist, and thus, compensation of the PA nonlinearity impact is visible. DFT-s-OFDM waveform generation practically matches that of the CP-OFDM waveform, with the key difference being an additional DFT operation prior to the subcarrier mapping and the main IFFT operation [16]. The additional DFT is usually referred to as transform precoding.

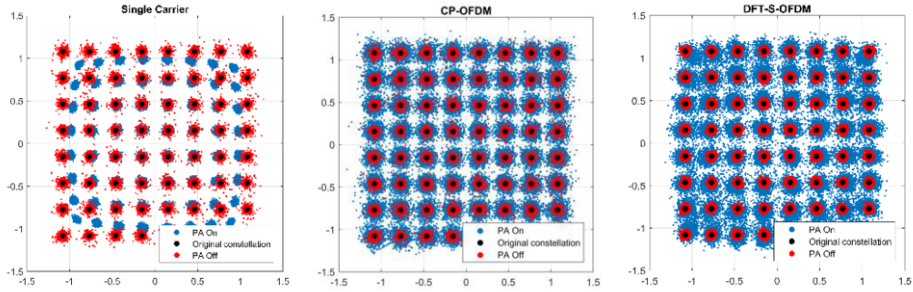

Figure 2. Examples of different constellation distortions on the receiver due to PA nonlinearity impact at the transmitter.

Two different approaches for PA nonlinearity mitigation have been proposed so far. The first is PA pre-distortion at the transmitter side, with preparation of the TX signals in such a way that minimizes PA nonlinearity negative effects. There are a number of such approaches, however they have a limited performance impact, and pre-distortion tends to have a poor performance at low input back-off (IBO) values [5-7]. Pre-distortion is also unavailable in small, low-cost devices like sensors, as it increases processing complexity and power consumption at the TX side.

Another way is the compensation of PA nonlinearity at the receiver. In paper [8], statistical processing of the received signals for the evaluation of the average PA distortion for further compensation was proposed. Works [5, 6, 9-11, 17, 18] considered a theoretical approach for PA nonlinearity compensation at the receiver side from a general point of view. In these papers a number of methods have been presented

for simple single carrier waveforms [5, 6, 9, 10], including hard-decision feedback, usage of the sequential Monte-Carlo method and inverse PA function. Several methods of the RX side nonlinearity compensation were considered for OFDM waveforms [11, 17, 18]. Therein, PA nonlinear distortion is represented as constant complex gain and a Gaussian noise component, with the main goal to obtain PA parameters (known or estimated with pilot signals) to compensate for the nonlinear distortion. In some papers [9-11] PA parameters are assumed to be known at the receiver to perform nonlinearity impact compensation. It is obvious that in cases when PA parameters need to be estimated, the system performance should be worse or at the same level.

3. Proposed RX-Side Compensation Approach

As it was shown for the SC modulations and, most importantly, in the DFT-s-OFDM case, the PA distortion has some deterministic component in addition to the ICI. With the knowledge of the TX PA nonlinearity function at the RX side, it is possible to compensate the deterministic component and thereby to improve the signal demodulation performance. This can be done by applying the RX processing, which is equivalent to the inverse function of the PA nonlinearity.

Generally, this function is not known at the receiver, not only because the PA characteristics are not known, but also due to the different TX power. The actual value of the TX power determines the working point of the PA and, thus, nonlinear distortions of the signal.

In several works, like [10, 11, 17], the decision-directed feedback is used for estimation of the power amplifier characteristics. Similarly, in [8] statistical processing is applied to adjust the demodulation algorithm to the received distorted signal. However, it is more effective to know the TX PA nonlinearity function and the working point for applying more precise inverse processing.

In this paper we present a receiver-side PA nonlinearity compensation method for the CP-OFDM and DFT-s-OFDM waveforms, based on usage of reverse signal processing, including an inverse PA distortion function. The communication system flow with PA compensation scheme (see Figure 3) consists of the basic TX processing at the transmitter side (1) that may include MIMO precoding and transform precoding (in the case of DFT-s-OFDM waveform), as well as standard OFDM IFFT block. The generated OFDM baseband signal is fed to one or more TX chains that may include CP insertion and frequency up conversion and finally come to the output power amplifiers (PAs) (2) operating at the carrier frequency. It should be noted, that for proper work of the proposed scheme, the signals on the different antennas should have the same amplitudes (but may have different phases). This limits the scheme's applicability to rank 1 (one data stream) transmission, even if several TX antennas are used. After propagating through the wireless channel, the signal comes to the RX chains (3) of one or more receive antennas for further baseline RX processing (4) that may consist of the FFT with maximum ration combining (MRC), frequency domain (FD) equalization, and inverse transform precoding (in the case of DFT-s-OFDM waveform). Such processing effectively removes the impact of the frequency selective channel, and we may use this signal in the PA distortion compensation block (5). This block may consist of the IFFT operation (6) for returning the signal into the time domain (TD), the Inverse PA nonlinear function block (7) that actually performs the PA nonlinearity compensation, and an FFT block to return the compensated signal back to the FD. In

the case of DFT-s-OFDM modulation, additional transform precoding blocks (9) and (10) are used for proper signal processing.

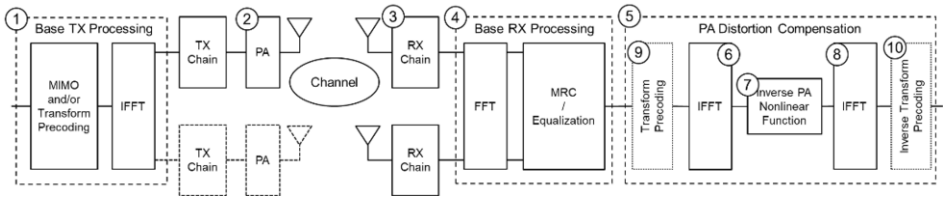

Figure 3. Schematic representation of the proposed receiver-side PA nonlinearity compensation scheme.

The inverse PA nonlinear function, which the signal is passed through inside of block (7), is obtained as an inverse of the Rapp AM-AM distortion in Eq. (1) with function value restrained, and is given in Eq. (2).

$$F^{-1}{}_{AM-AM}(x) = \begin{cases} \dfrac{x}{\left(1-\left|\dfrac{x}{V_{sat}}\right|^{2p}\right)^{\frac{1}{2p}}}, x < \alpha V_{sat} \\ \dfrac{\alpha V_{sat}}{(1-|\alpha|^{2p})^{\frac{1}{2p}}}, x \geq \alpha V_{sat} \end{cases}, \quad (2)$$

where $F^{-1}{}_{AM-AM}$ is the inverse amplitude distortion function, α is a border-setting coefficient, which is required to prevent the function $F^{-1}{}_{AM-AM}$ from reaching infinity at $x = V_{sat}$. The value of the coefficient α, used in the simulations, was $\alpha = 0.9$. It should be noted that it is important to constrain the inverse function with some ceiling, since allowing it to reach infinity may cause even more distortion to occur at the output of the compensation scheme.

4. Simulation Results

To prove the feasibility of the proposed approach for the receiver-side PA nonlinearity compensation method, link-layer simulations (LLS) were performed, comparing the proposed scheme with the cases of ideal PA and an uncompensated case for a given PA model. The PA model based on the parameters of the typical real power amplifiers in the 30-70 GHz band [13] was used, along with a newly developed PA model for the 100-200 GHz (see Table 1). Simulations were performed for different system parameters, such as subcarrier spacing (SCS), used waveform type, coding and modulation scheme, etc. The full list of LLS simulation parameters is summarized in Table 2. Simulation results, the block error rate (BLER) vs. signal-to-noise ratio (SNR), for the 30-70 GHz PA model are shown in Figures 4-6, and for the 100-200 GHz PA model in Figures 7-9.

To make an apple-to-apple system comparison, we have fixed the bandwidth (BW) to be 400 MHz. It leads to a change in the amount of resource blocks (RB) being used

in one slot in a simulation, depending on the SCS. The larger the SCS, the less RBs we can get for the given BW.

In the case of DFT-s-OFDM, transform precoding has been performed on the data-carrying subcarriers, which differs from the main IFFT. For example, if data is allocated into $N_{RB} = 64$ RBs, then the transform precoding DFT is performed on $N_{RB} \cdot 12 = 768$ subcarriers, whereas the main OFDM IFFT operation is performed on the closest power of 2 to the number of data subcarriers, in this case - 1024 subcarriers.

Table 2. System parameters and simulation assumptions.

Parameters	Assumption
Carrier Frequency	60 GHz / 180 GHz
Bandwidth	400 MHz
Waveform	CP-OFDM, CP-DFT-s-OFDM
PA Model & Parameters	30-70 GHz PA model [13], 100-200 GHz PA derived model
TX power	10 dBm
SCS	120 kHz / 480 kHz / 960 kHz
Resource blocks allocated	256 / 64 / 32 RBs
Channel Model	TDL-A, 5ns DS, 3 km/h (Doppler $f_D = 167$ Hz)
Transmission scheme	1x2 MRC
Modulation and coding	64-QAM, R=0.65 (MCS 22 Table 1) [19] 64-QAM, R=0.89 (MCS 27 Table 1) [19] 256-QAM, R=0.74 (MCS 22 Table 2) [19]
Impairments	Phase noise (BS and UE example 2 model, [20]), compensated with LS filter Channel estimation: LS fitting per precoding region (24 subcarriers)

4.1. Simulation Results for 30-70 GHz PA Model

Simulation results obtained for the 30-70 GHz PA model show that with the addition of the nonlinear PA, the performance decreases as expected. The use of the described algorithm improves the BLER metrics, compared with the uncompensated case for both CP-OFDM and DFT-s-OFDM waveforms.

For the SCS 960 kHz and 480 kHz (Figures 4, 5), the gain in performance can reach 3-5 dB on average. Since CP-OFDM has a greater PAPR value than that of DFT-s-OFDM, the performance drop from the PA nonlinearity for the CP-OFDM is much more noticeable compared to DFT-s-OFDM. Moreover, for considered impairments (PN + the PA nonlinearity) the 256-QAM modulation (MCS 22 T2) cannot be used for the CP-OFDM system at all.

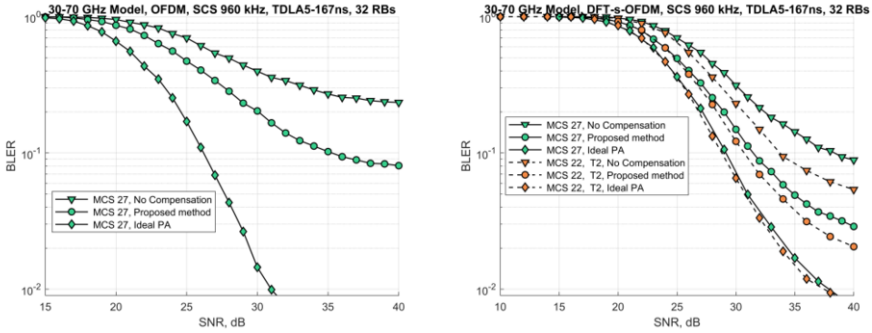

Figure 4. BLER for SCS 960 kHz, 64-QAM/256 QAM for OFDM (left) and DFT-s-OFDM (right).

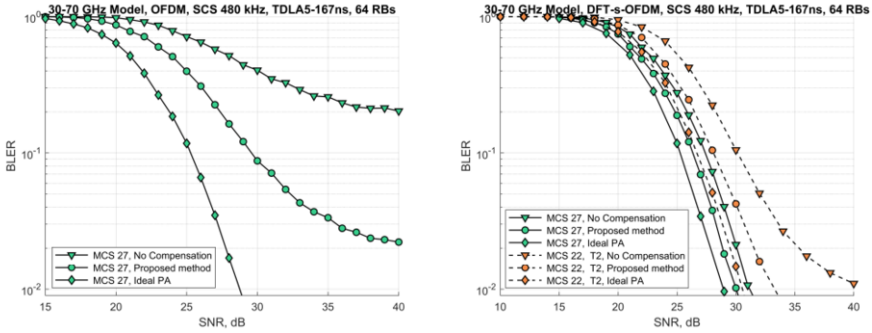

Figure 5. BLER for SCS 480 kHz, 64-QAM/256 QAM for OFDM (left) and DFT-s-OFDM (right).

As shown in [21], for the lower values of the SCS (15-120 kHz) the phase noise (PN) plays a dominant part in the system performance degradation due to the higher inter-carrier interference (ICI). That leads to a decrease of the PA nonlinearity impact on the whole system performance and, consequently, on the effectiveness of any PA nonlinearity compensation scheme. This effect is demonstrated in Figure 6 for both CP-OFDM and DFT-s-OFDM systems with SCS 120 kHz.

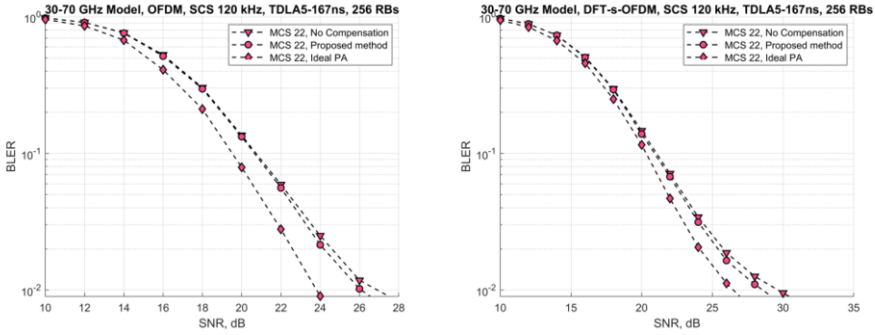

Figure 6. BLER for SCS 120 kHz, 64-QAM for OFDM (left) and DFT-s-OFDM (right).

4.2. Simulation Results for 100-200 GHz PA Model

For the derived 100-200 GHz PA model, the effects of the additional nonlinear distortion are even more pronounced (Figures 7-9). In this sub-THz band, most of the 256-QAM (MCS 22 Table 2) simulation results have ended up being unusable – the amount of errors in the data has reached a point, where the data is basically unrecoverable. Since the effect of the PA impairment has increased, the impact of the PN is now less dominant, which allows for the PA compensation schemes to be more effective.

For the CP-OFDM case, the increase of the PA nonlinearity effect allows for compensation to provide the desired performance gain for MCS 22 (Figure 7, left).

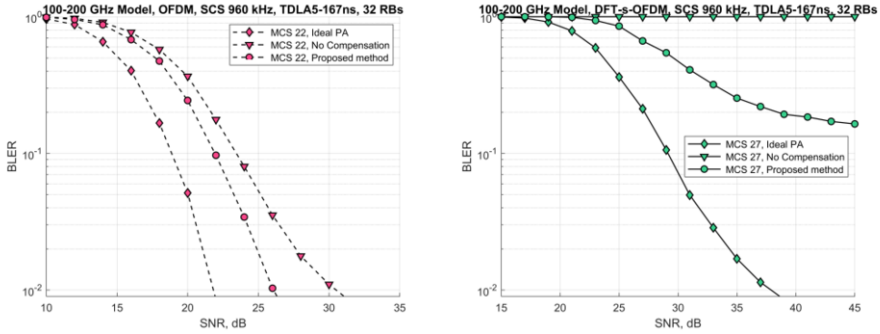

Figure 7. BLER for SCS 960 kHz, 64-QAM for OFDM (left) and DFT-s-OFDM (right).

For the DFT-s-OFDM with SCS 960 kHz (Figure 7, right), the PA nonlinearity has caused a significant decrease in performance to the point of data loss. The proposed compensation scheme has eliminated distortions in the received information and removed the BLER floor effect for MCS 27.

Figure 8 demonstrates similar system performances for the CP-OFDM and the DFT-s-OFDM cases for SCS 480 kHz.

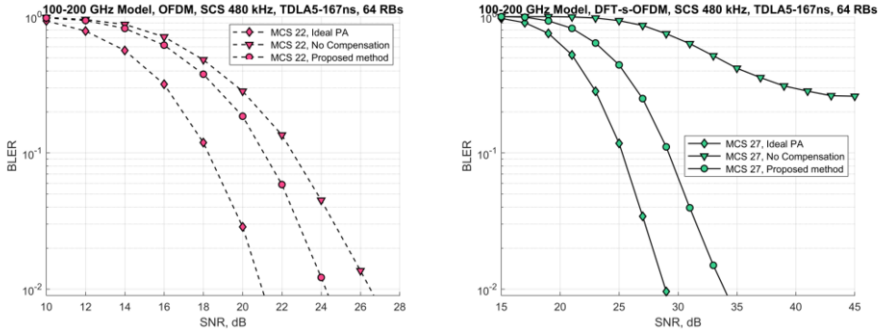

Figure 8. BLER for SCS 480 kHz, 64-QAM for OFDM (left) and DFT-s-OFDM (right).

For the CP-OFDM SCS 120 kHz (Figure 9, left), the effect of the PA nonlinearity is now more significant, and has a greater impact on the performance compared to the PN. This allows effective application of the proposed compensation scheme, since the system performance decrease is mostly related to the PA nonlinearity, and is slightly affected by the PN. DFT-s-OFDM is less affected by the PA nonlinearity due to low PAPR, and the PN is still the dominant impairment in that case (see Figure 9, right).

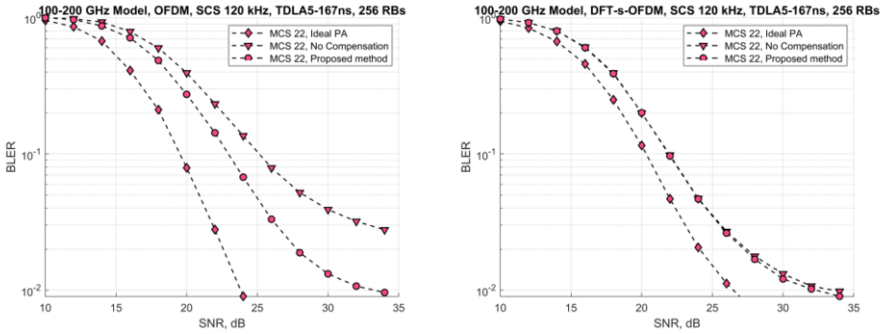

Figure 9. BLER for SCS 120 kHz, 64-QAM for OFDM (left) and DFT-s-OFDM (right).

4.3. Discussions

For the 30-70 GHz PA model analysis, the proposed PA nonlinearity compensation scheme demonstrates system improvement for the high modulations and coding schemes. For the SCS 960 kHz and 480 kHz, where the PN impact is non-dominant, the effect of the PA becomes the main system performance limiting factor and application of the proposed compensation scheme may provide several dB gain or even mitigate the BLER floor effect. For the SCS 120 kHz, the negative effect of the PN is dominant, and the use of any PA nonlinearity compensation scheme is not effective.

For the 100-200 GHz PA model, the impact of the PA nonlinearity increases considerably. Therefore, application of the proposed compensation scheme for 64-QAM modulation - MCS 22 and MCS 27 has shown a noticeable performance improvement compared with the uncompensated results. In several cases, the proposed compensation algorithm has even restored the data from being unusable and considerably improved the communication system performance. It should also be noted that in that case PN plays a less dominant role, allowing for efficient PA nonlinearity compensation at lower SCS values, like 120 kHz.

5. Conclusion

A method for compensation of the TX PA nonlinear distortion at the receiver side has been presented. The method at its core is based on the use of an inverse PA's distortion curve for compensation, it can be applied to different waveform types and can be adjusted for the task at hand. The method has been implemented and tested in a fully-fledged 5G NR link-level simulator for performance evaluation. Performance has been measured for the existing 30-70 GHz PA model, as well as a newly developed 100-200 GHz PA model, based on available recent research results. In both cases, the proposed method has shown the ability to significantly improve system performance in various scenarios (waveform, QAM constellation, PA model). As the method relies on ~~the~~ receiver-side compensation, this approach can be useful for communication systems with a large number of low-cost devices which use energy-efficient simple transmitters (e.g. in IoT case). This would allow the transmitter power consumption to be reduced

since there is no need to apply any kind of preprocessing for PA's nonlinearity compensation at the TX side.

References

[1] 3GPP. Study on NR beyond 52.6 GHz. 3rd Generation Partnership Project (3GPP); 2019. 38.807. Version 1.0.0.

[2] Intel Corporation. New SID: Study on supporting NR from 52.6GHz to 71 GHz. 3rd Generation Partnership Project (3GPP); 2019. RP-193259. TSG RAN Meeting №86.

[3] Qualcomm. New WID on extending current NR operation to 71 GHz. 3rd Generation Partnership Project (3GPP); 2019. RP-193229. TSG RAN Meeting №86.

[4] Zhang J, Wu T, Nie L, Ma S, Chen Y, Ren J. A 120–150 GHz Power Amplifier in 28-nm CMOS Achieving 21.9-dB Gain and 11.8-dBm P_sat for Sub-THz Imaging System. IEEE Access. 2021; 9: 74752-62.

[5] Sharath M. Analysis and Compensation of Power Amplifier Distortions in Wireless Communication Systems [Ph.D. thesis]; 2015. Electronic Thesis and Dissertation Repository.

[6] Shabany M, Gulak PG. Efficient Compensation of the Nonlinearity of Solid-State Power Amplifiers Using Adaptive Sequential Monte Carlo Methods. IEEE Transactions on Circuits and Systems I: Regular Papers. 2008; 55(10):3270-83.

[7] Eda T, Ito T, Ohmori H, Sano A. Adaptive Compensation of Nonlinearity in High Power Amplifier by Support Vector Machine. IFAC Proceedings Volumes. 2001; 34(14):243-8. IFAC Workshop on Adaptation and Learning in Control and Signal Processing (ALCOSP 2001), Cernobbio-Como, Italy, 29-31 August 2001.

[8] Ermolaev GA, Bolkhovskaya OV, Maltsev AA. Advanced Approach for TX Impairments Compensation Based on Signal Statistical Analysis at the RX Side. In: 2021 Wave Electronics and its Application in Information and Telecommunication Systems (WECONF); 2021. p. 1-5.

[9] Bhat S, Chockalingam A. Compensation of power amplifier nonlinear distortion in spatial modulation systems. In: 2016 IEEE 17th International Workshop on Signal Processing Advances in Wireless Communications (SPAWC); 2016. p. 1-6.

[10] Qi J, Aissa S. Analysis and Compensation of Power Amplifier Nonlinearity in MIMO Transmit Diversity Systems. IEEE Transactions on Vehicular Technology. 2010; 59(6):2921-31.

[11] Gregorio F, Werner S, Laakso TI, Cousseau J. Receiver Cancellation Technique for Nonlinear Power Amplifier Distortion in SDMA–OFDM Systems. IEEE Transactions on Vehicular Technology. 2007;56(5):2499-516.

[12] Rapp C. Effects of HPA-nonlinearity on 4-DPSK/OFDM-signal for a digital sound broadcasting system; 1991. p. 179-184.

[13] Nokia. Realistic power amplifier model for the New Radio evaluation. 3rd Generation Partnership Project (3GPP); 2016. R4-163314. TSG-RAN WG4 Meeting №79.

[14] Amado Rey AB. Analysis, design, and experimental evaluation of sub-THz power amplifiers based on GaAs metamorphic HEMT technology [Ph.D. thesis]; 2018.

[15] Ali A, Yun J, Giannini F, Ng HJ, Kissinger D, Colantonio P. 168-195 GHz Power Amplifier With Output Power Larger Than 18 dBm in BiCMOS Technology. IEEE Access. 2020; 8:79299-309.

[16] Chen X, Cui J, Ni W, Wang X, Zhu Y, Zhang J, et al. DFT-s-OFDM: Enabling Flexibility in Frequency Selectivity and Multiuser Diversity for 5G. IEEE Consumer Electronics Magazine. 2020;9(6):15-22.

[17] Bouhadda H, Zayani R, Shaiek H, Roviras D, Bouallegue R. Receiver Technique for Detection and Correction of Nonlinear High Power Amplifier Distortion Errors in OFDM Systems. In: 2015 IEEE 81st Vehicular Technology Conference (VTC Spring); 2015. p. 1-5.

[18] Drotar P, Gazda J, Deumal M, Galajda P, Kocur D. Receiver based compensation of nonlinear distortion in MIMO-OFDM. In: 2010 IEEE International Microwave Workshop Series on RF Front-ends for Software Defined and Cognitive Radio Solutions (IMWS); 2010. p. 1-4.

[19] 3GPP. Physical layer procedures for data. 3rd Generation Partnership Project (3GPP); 2020. 38.214. Version 16.2.0.

[20] 3GPP. Study on new radio access technology: Radio Frequency (RF) and co-existence aspects. 3rd Generation Partnership Project (3GPP); 2017. 38.803. Version 14.2.0.

[21] Maltsev A, Pudeev A, Kim S, Yang S, Choi S, Myung S. Phase Tracking Sequences for 5G NR in 52.6-71 GHz Band: Design and Analysis. Proceedings of CECNet 2021. 2021.